NRL Report 8700

A Matched Filter Doppler Processor for Airborne Radar

G. A. ANDREWS AND S. L. SHELLER

Airborne Radar Branch
Radar Division

July 13, 1983

NAVAL RESEARCH LABORATORY
Washington, D.C.

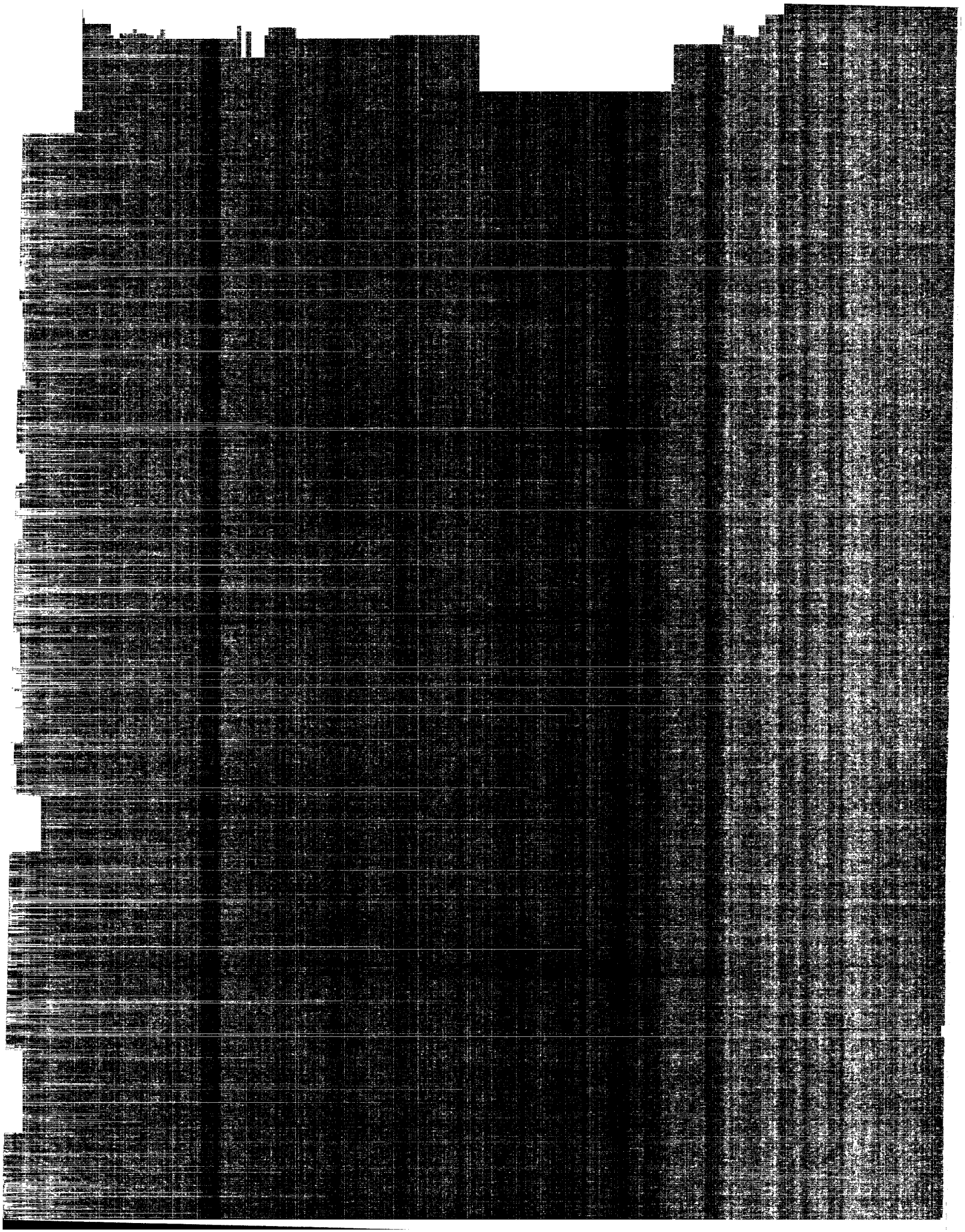

SECURITY CLASSIFICATION OF THIS PAGE *(When Data Entered)*

REPORT DOCUMENTATION PAGE		READ INSTRUCTIONS BEFORE COMPLETING FORM
1. REPORT NUMBER NRL Report 8700	2. GOVT ACCESSION NO.	3. RECIPIENT'S CATALOG NUMBER
4. TITLE *(and Subtitle)* A MATCHED FILTER DOPPLER PROCESSOR FOR AIRBORNE RADAR		5. TYPE OF REPORT & PERIOD COVERED Interim report on a continuing NRL problem 6. PERFORMING ORG. REPORT NUMBER
7. AUTHOR*(s)* G. A. Andrews and S. Sheller		8. CONTRACT OR GRANT NUMBER*(s)*
9. PERFORMING ORGANIZATION NAME AND ADDRESS Naval Research Laboratory Washington, DC 20375		10. PROGRAM ELEMENT, PROJECT, TASK AREA & WORK UNIT NUMBERS 62712N,XF12-141-000 53-1854-00 62712N,WF12-100-000 53-0662-00
11. CONTROLLING OFFICE NAME AND ADDRESS Naval Electronics Systems Command Washington, DC 20360 and Naval Air Systems Command Washington, DC 20361		12. REPORT DATE July 13, 1983 13. NUMBER OF PAGES 28
14. MONITORING AGENCY NAME & ADDRESS*(if different from Controlling Office)*		15. SECURITY CLASS. *(of this report)* UNCLASSIFIED 15a. DECLASSIFICATION/DOWNGRADING SCHEDULE

16. DISTRIBUTION STATEMENT *(of this Report)*

Approved for public release; distribution unlimited.

17. DISTRIBUTION STATEMENT *(of the abstract entered in Block 20, if different from Report)*

18. SUPPLEMENTARY NOTES

19. KEY WORDS *(Continue on reverse side if necessary and identify by block number)*

Moving target indicator (MTI)
Antenna pattern
Minimum detectable velocity (MDV)
Doppler filtering
Motion compensation
Time averaged clutter coherent airborne radar (TACCAR)
Displaced phase center antenna (DPCA)
Fast Fourier transform (FFT)

20. ABSTRACT *(Continue on reverse side if necessary and identify by block number)*

The airborne radar presents noteworthy problems of clutter cancellation because of platform motion. The returns from fixed objects must be filtered out as clutter. A matched filter signal processor design is presented that produces the necessary level of clutter rejection. The results are compared to various processor configurations, e.g., moving target indicators (MTIs) cascaded with a matched filter processor, displaced phase center antenna (DPCA) cascaded with a matched

(Continued)

DD FORM 1 JAN 73 1473 EDITION OF 1 NOV 65 IS OBSOLETE
S/N 0102-014-6601

SECURITY CLASSIFICATION OF THIS PAGE *(When Data Entered)*

20. ABSTRACT (Continued)

filter processor, the fast Fourier transform (FFT), and MTIs cascaded with the FFT. The processors are compared on the basis of their clutter rejection, signal processing losses, and minimum detectable velocity (MDV) capabilities.

CONTENTS

A MATCHED FILTER DOPPLER PROCESSOR FOR AIRBORNE RADAR

INTRODUCTION

Two complications inherent in the detection of aircraft from an airborne moving platform are the level of clutter rejection required (70 dB or better is the goal in this research) and the difficulties arising from the platform motion which both shifts the clutter spectrum and increases its width.

Another problem with Doppler frequency processing is the minimum detectable velocity (MDV), which introduces blind regions in the surveillance region. The width of the blind region is directly related to the MDV (i.e., the higher the MDV the wider the blind region). Because of such blind regions, there exists the possibility of a target penetrating a surveillance region by flying a course that is nearly tangential to the radar platform.

In the research reported here, it is shown that a matched filter signal process or [1] will produce the necessary level of clutter rejection to distinguish moving from fixed targets. The results are compared to those obtained using a fast Fourier transform (FFT) processor and with those obtained using a moving target indicator (MTI) cascaded with an FFT Doppler filter bank [2].

THE MATCHED FILTER CONCEPT

Applebaum's adaptive-antenna algorithm [3] can be applied to the control of a bank of Doppler filters [4]. From [3] and [4] the optimum filter weight vector for a matched filter (i.e., when the signal is known completely so that the signal vector S can be defined) is

$$W_{\text{opt}} = M_I^{-1} S^*, \tag{1}$$

where M_I^{-1} represents the inverse interference covariance matrix and the superscript (*) denotes the complex conjugate.

In [1] a generalized filter is derived by assuming that the signal's Doppler shift is not precisely known but is known only within some interval. The entire Doppler region of interest is covered with a bank of filters, one for each interval.

For very small pulse widths compared to the time between pulses [5], the received signal has the form

$$s(t) = \delta(t - kT) \exp(j2\pi f_d t), \tag{2}$$

where T is the time between transmitted pulses,

$$k \in \{\text{integers}\}, \text{ and } \delta(t - kT) = \begin{cases} 0, & t \neq kT \\ 1, & t = kT. \end{cases}$$

Assuming the Doppler shift f_d has a uniform probability density function over an interval of length B centered at f_i, then

Manuscript approved January 27, 1983.

$$P(f_d) = \begin{cases} \dfrac{1}{B}, & f_i - \dfrac{B}{2} \leqslant f_d < f_i + \dfrac{B}{2} \\ 0, & \text{elsewhere,} \end{cases} \tag{3}$$

where f_i is the center of the ith filter and is given by $f_i = (i-1)/NT$, $i = 1, 2, \ldots, N$ and $B = 1/NT$ where N is the number of pulses integrated.

Figure 1 (using an 8-pulse processor as an example) shows the principal difference between the Applebaum algorithm and the design presented in [1] and applied here to an airborne system. In Fig. 1a each filter is optimized (i.e., matched) to one particular Doppler frequency. In Fig. 1b, the design used here, the filter is optimized to detect moving targets that have Doppler frequencies that fall anywhere within one of the intervals (i.e., it is matched to the expected value). Thus, f_i represents the center of the ith filter with the first filter centered on zero Doppler as shown in Fig. 1.

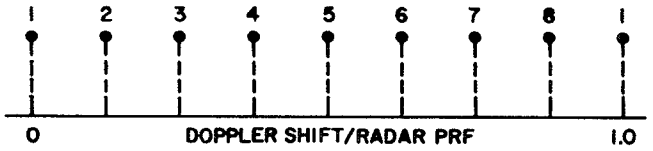

(a) Equally spaced points

(b) MTI detection region

Fig. 1 — Basis for the design of a bank of filters to reject the clutter and detect a target with (a) a Doppler shift at one of the equally spaced points or with (b) a Doppler shift that may be anywhere within one of the equal intervals of the MTI detection region

The expectation of the signal with respect to the unknown Doppler shift is

$$\bar{s}(t) = E\{s(t)\} = \delta(t - kT) \int_{-\infty}^{\infty} P(f_d) \exp(j2\pi f_d t)\, df_d.$$

The integral above is the inverse Fourier transform of the probability density function of the Doppler shift which yields

$$\bar{s}(t) = \delta(t - kT) \exp(j2\pi f_i t) \frac{\sin(\pi Bt)}{\pi Bt}. \tag{4}$$

All the parameters of Eq. (4) are known except k.

An N-pulse Doppler filter requires N samples of $\bar{s}(t)$. We must choose N sequential samples from the infinite set described by Eq. (4). The filter response to $\bar{s}(t)$ is maximized if the samples selected are centered around the peak of the $(\sin x)/x$ curve of Eq. (4).

The lth component of the signal vector for the ith filter is

$$\bar{s}_l = \exp\left[j\,\frac{2\pi(i-1)}{N}\left(l-\frac{N+1}{2}\right)\right]\;\frac{\sin\left[\frac{\pi}{N}\left(l-\frac{N+1}{2}\right)\right]}{\frac{\pi}{N}\left(l-\frac{N+1}{2}\right)} \tag{5}$$

for $l = 1, 2, \ldots, N$ and $i = 1, 2, \ldots, N$.

Since Eq. (5) represents a completely known signal vector, it can be used in the Applebaum algorithm

$$W_{\text{opt}} = M_I^{-1}\,\bar{S}^* \tag{6}$$

where the lth component of $\bar{S}^*$ is given by the complex conjugate of Eq. (5). By using the expected value of the signal rather than the known value, we do not have a matched filter in the strict meaning of the phrase. What we actually have is a filter matched to the expected value of the unknown signal vector. Therefore, weight vectors can be computed by using Eq. (6).

One then determines the platform motion spectrum. The platform motion spectrum (Fig. 2) consists of samples that are computed from the gain of the antenna pattern at a given angle relative to boresight multiplied by the backscatter of the clutter taken in equal steps of frequency (not angle) and converted to the azimuth angle.

For a 0° dive angle, applying Eq. (A3) gives,

$$f_d = \frac{2v_p}{\lambda}\cos\phi\,\cos\alpha \tag{7}$$

where ϕ is the depression angle of the antenna relative to the velocity ($\vec{v}_p$) and α is the azimuth.

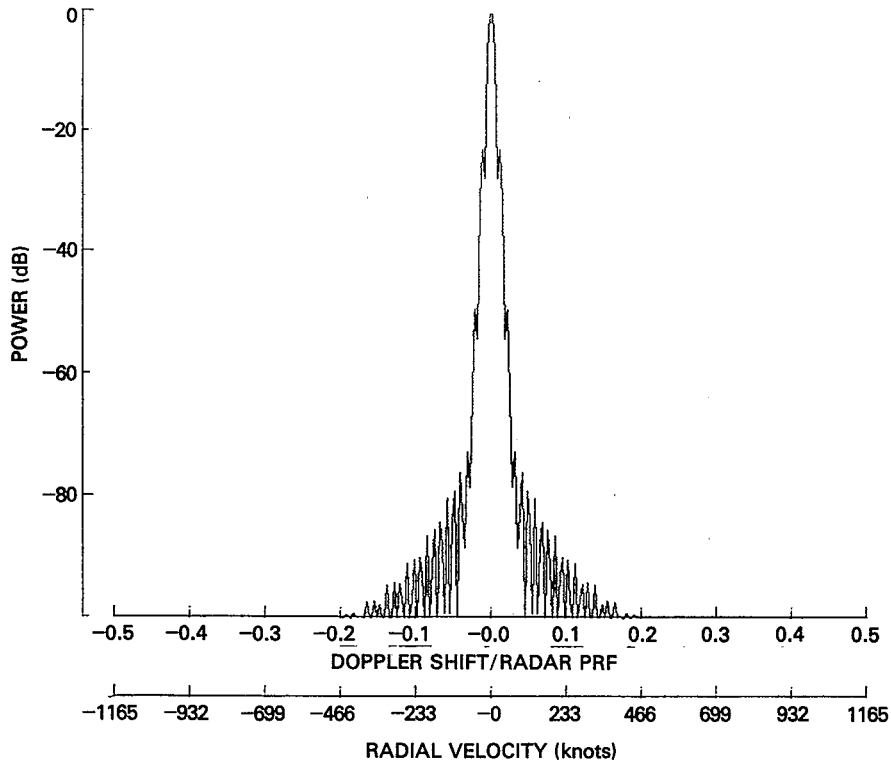

Fig. 2 — Clutter spectrum due to platform motion; 5 nmi (30 000 ft) altitude, 50-kHz pulse repetition frequency, azimuth is 90°

By Eq. (7),

$$f_a + n\Delta f_d = \frac{2v_p}{\lambda} \cos\phi \cos(\alpha_a + \alpha_n) \tag{8}$$

where α_a is the azimuth of boresight relative to the velocity, f_a is the Doppler frequency on boresight, n is an integer representing the number of equal frequency steps with respect to boresight, and α_n is the azimuth (relative to boresight) corresponding to the frequency represented by the left-hand side.

Solving Eq. (8) for α_n we get

$$\alpha_n = \cos^{-1}\left[\frac{(f_a + n\Delta f_d)\lambda}{2v_p \cos\phi}\right] - \alpha_a.$$

If we let $\kappa = \dfrac{\lambda}{2v_p \cos\phi}$, then

$$\alpha_n = \cos^{-1}[(f_a + n\Delta f_d)\kappa] - \alpha_a, \tag{9}$$

where $n = -n_{\min}, \ldots, -2, -1, 0, 1, 2, \ldots, n_{\max}$.

Choosing a Δf_d to assure an adequate number of points, we determine both $n_{\min}$ such that

$$f_a - n_{\min}\Delta f_d \geqslant -\frac{2v_p}{\lambda} \cos\phi, \tag{10}$$

and $n_{\max}$ such that

$$f_a + n_{\max}\Delta f_d \leqslant \frac{2v_p}{\lambda} \cos\phi. \tag{11}$$

$n_{\min} \neq n_{\max}$ except where $\alpha_a = 90°$.

The total number of points for a given ϕ and α_a is

$$n = n_{\min} + n_{\max} + 1. \tag{12}$$

Thus, we can determine the azimuth angles with respect to boresight by Eq. (9), e.g.,

$$\alpha_{\min} = \cos^{-1}[(f_a - n_{\min}\Delta f_d)\kappa] - \alpha_a$$

$$\vdots$$

$$\alpha_{-2} = \cos^{-1}[(f_a - 2\Delta f_d)\kappa] - \alpha_a$$

$$\alpha_{-1} = \cos^{-1}[(f_a - 1\Delta f_d)\kappa] - \alpha_a$$

$$\alpha_0 = \cos^{-1}[(f_a + 0\Delta f_d)\kappa] - \alpha_a \quad \text{(boresight)}$$

$$\alpha_1 = \cos^{-1}[(f_a + 1\Delta f_d)\kappa] - \alpha_a$$

$$\alpha_2 = \cos^{-1}[(f_a + 2\Delta f_d)\kappa] - \alpha_a$$

$$\vdots$$

$$\alpha_{\max} = \cos^{-1}[(f_a + n_{\max}\Delta f_d)\kappa] - \alpha_a$$

where α_{min} represents the azimuth angle (relative to boresight) where the minimum Doppler frequency $\geqslant -2v_p/\lambda \cos \phi$ occurs, α_{max} represents the azimuth angle (relative to boresight) where the maximum Doppler frequency $\leqslant 2v_p/\lambda \cos \phi$ occurs, and the other subscripts designate the azimuth angles (relative to boresight) corresponding to the equivalent number of frequency steps with respect to boresight (0 for boresight, negative for frequencies less than boresight, and positive for frequencies greater than boresight).

Next, to determine the area of the clutter for each sample, apply

$$A_c = \frac{c\tau}{2} \sec \psi \left[2R \tan \left[\frac{\Delta\theta}{2}\right]\right], \tag{13}$$

where R is the slant range corresponding to the depression angle ϕ, ψ is the grazing angle, c is the propagation speed, τ is the pulse width, and $\Delta\theta$ is a function of α.

$\Delta\theta$ is computed by one-half the sum of the two angular widths (angular widths are determined by subtracting each consecutive pair of results from Eq. (9)) adjacent to an azimuth angle computed by Eq. (9).

Finally,

$$\sigma_c = A_c \sigma^0. \tag{14}$$

A similar procedure is performed in the Appendix for filter widths and the area of the clutter for the footprint. The variation of azimuth angular widths when equal frequency steps are used can be seen clearly in Fig. (A2). However, the frequency steps used in the Appendix are not the same as those applied here. Here, we require a relatively large number of points (i.e., much smaller Δf_ds).

The interference spectral density due to internal motion (the clutter has a Gaussian frequency spectrum; the noise has a "white" frequency spectrum; the clutter and noise both have a Gaussian amplitude probability density function; normalized to unity $E_G + E_w = 1$) is given by

$$P_I(f_d) = \frac{1 - E_w}{\sqrt{2\pi}\,\sigma_c} \exp\left[-\frac{(f_d - \mu_c)^2}{2\,\sigma_c^2}\right] + E_w T \left[u(f_d) - u\left[f_d - \frac{1}{T}\right]\right], \tag{15}$$

where the mean μ_c implies relative motion between the radar platform and the clutter, σ_c (the standard deviation of the clutter spectrum) is a measure of the bandwidth of the clutter spectrum, T is the time between transmitted radar pulses, E_w is the power of the "white" spectrum E_G is the power of the Gaussian spectrum, and

$$u(f_d) = \begin{cases} 0, & f_d < 0 \\ 1, & f_d \geqslant 0. \end{cases}$$

The internal motion spectrum is computed by Eq. (15) by using the same frequency steps as one does in computing the platform motion spectrum.

The interference covariance matrix, M_I, may be determined by first convolving the spectrum of the internal motion plus noise (Eq. 15) with the platform motion spectrum (Fig. 2) to yield the total spectrum.

Second, take the inverse discrete Fourier transform of the total spectrum [5]. This produces a discrete autocorrelation of the delay (τ) where τ is defined by

$$\tau = nT, \; -N \leqslant n \leqslant N \text{ and } n \in \{\text{integers}\}. \tag{16}$$

Finally, the interference covariance matrix elements may be determined as presented in the Appendix of [5].

Matched Filter

Figure 3 shows the shape of filter number 33 of the matched filter processor with optimal weights defined by Eq. (6). The internal motion is small compared to the platform motion. Therefore, the filter is approximately matched to the platform motion spectrum of Fig. 2. The reciprocal relationship between the filter response of Fig. 3 and the spectrum of Fig. 2 can be seen. The loss is about 0.1 dB.

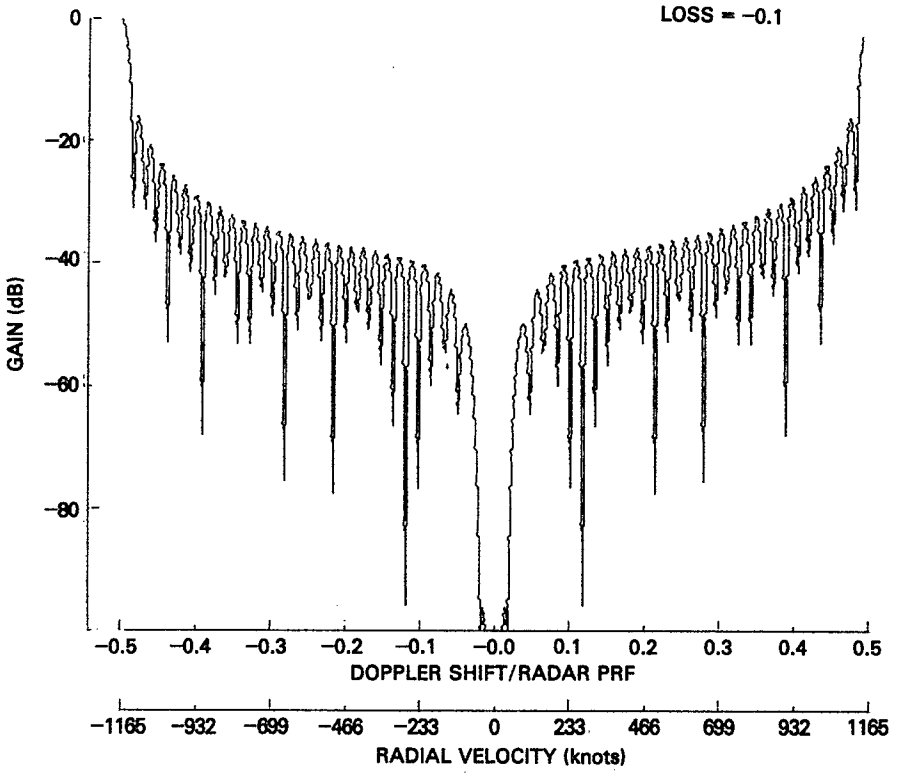

Fig. 3 — Filter No. 33 of a 64-pulse matched filter processor with optimal weights. This filter is optimized to the "input" spectrum of Fig. 2.

Figure 4 shows the improvement factor (IF) of the matched filter processor for this example. The clutter-to-noise ratio is 65 dB. The MDV is the velocity at which we can achieve a 70-dB improvement factor (explained later). For this processor it is about 80 knots.

Cascaded MTI and Matched Filter

For a cascaded MTI-Matched filter configuration, the filter is matched to the covariance matrix corresponding to the output spectrum shown in Fig. 5 which shows the results of a single MTI canceller (main lobe clutter is reduced by about 34 dB).

Figure 6 shows the IF for this processor with optimal weights defined by Eq. (6). The clutter-to-noise ratio is 65 dB. The MDV is about 80 knots and the loss is about 0.1 dB. The IF is about 5 dB less than shown in Fig. 4.

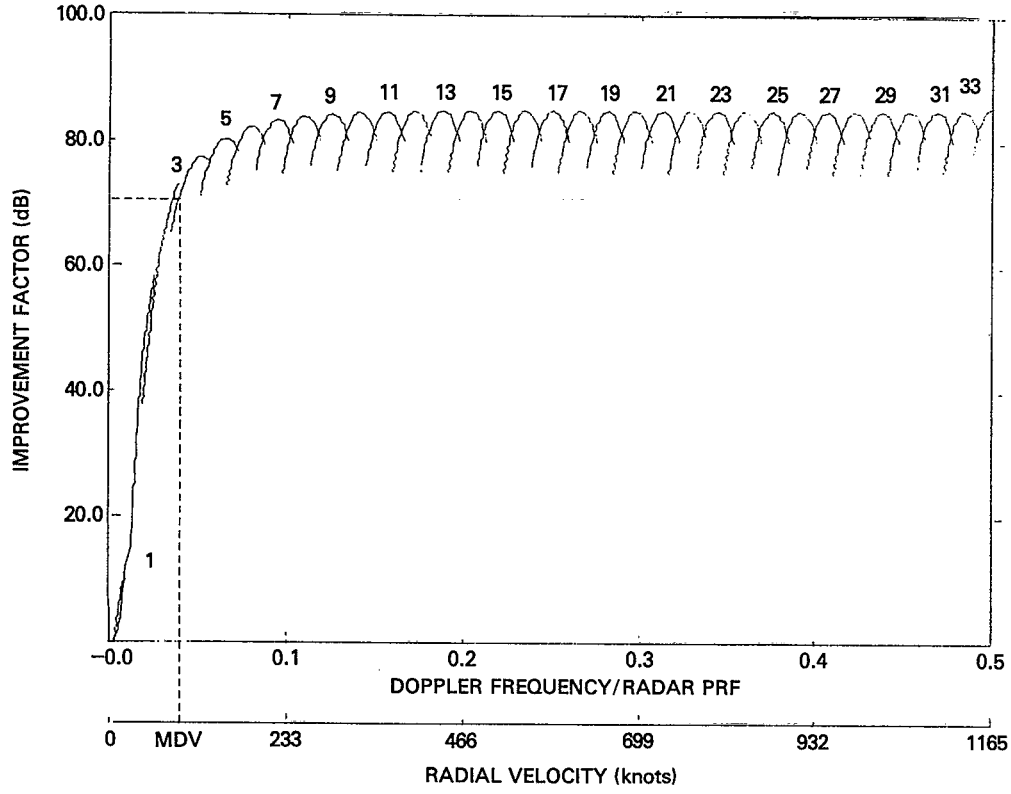

Fig. 4 — Improvement factor for a 64-pulse Doppler processor using the matched filter algorithm with optimal weights. The clutter-to-noise ratio is 65 dB.

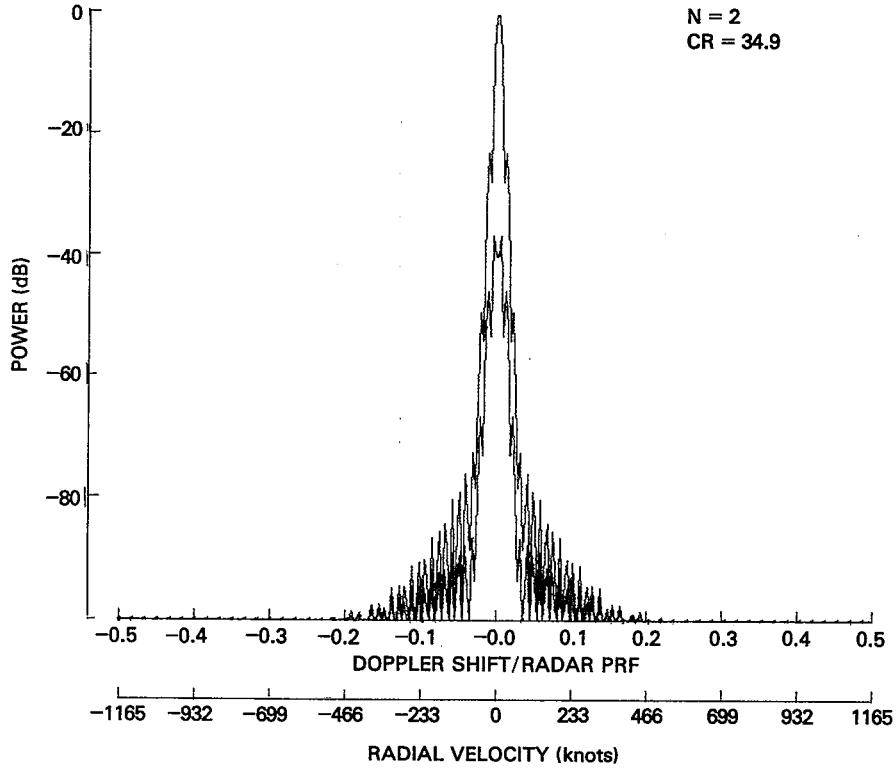

Fig. 5 — Single MTI canceller to reduce main lobe clutter

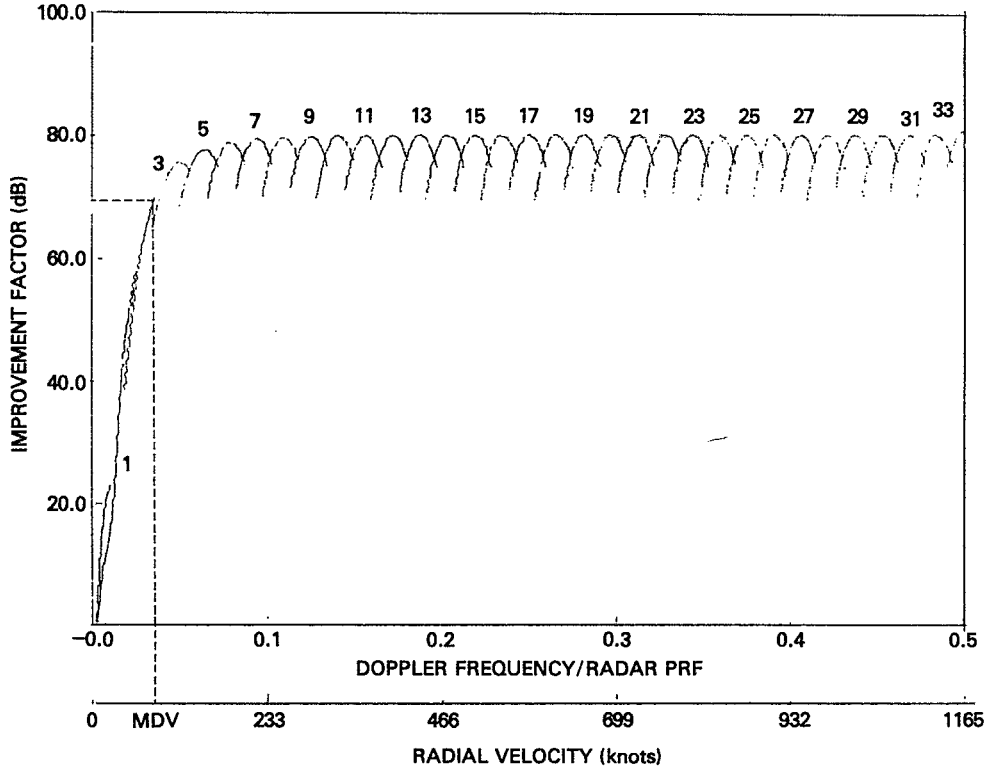

Fig. 6 — Improvement factor for a 64-pulse Doppler processor using the matched filter algorithm preceded by a single-canceller MTI. The clutter-to-noise ratio is 65 dB.

Since the matched filter without the MTI is a much simpler processor design and since there is no degradation of performance, it appears to be the better configuration. However, an MTI-matched filter system using a single-canceller requires about six bits less precision in the processor as shown by its cancellation ratio (CR on Fig. 5) of about 35 dB. This may be desirable for some applications because it would require less total hardware.

Cascaded DPCA Canceller and Matched Filter

Two commonly used methods of correcting for platform motion are time averaged clutter coherent airborne radar (TACCAR) and displaced phase center antenna (DPCA). TACCAR [6] removes the average Doppler shift due to platform motion, and DPCA [7] corrects for the spectral spreading also due to the platform motion. Figure 7 shows the results when a DPCA canceller is cascaded with a 64-pulse matched filter processor. The clutter-to-noise ratio is 65 dB. The IF is about the same as that shown in Fig. 4 for the matched filter alone. However, the MDV is about 45 knots *vs* about 80 knots. This is a remarkable improvement in the MDV. Although this processor requires less processing hardware for the same reason as the MTI, it introduces antenna complications in that usually three antenna patterns must be generated [7].

COMPARISON WITH OTHER TECHNIQUES

Current radar Doppler processing techniques to distinguish moving from fixed targets consist of:

1. The moving target indicator (MTI),
2. The weighted fast Fourier transform (FFT), and
3. The cascaded MTI/FFT.

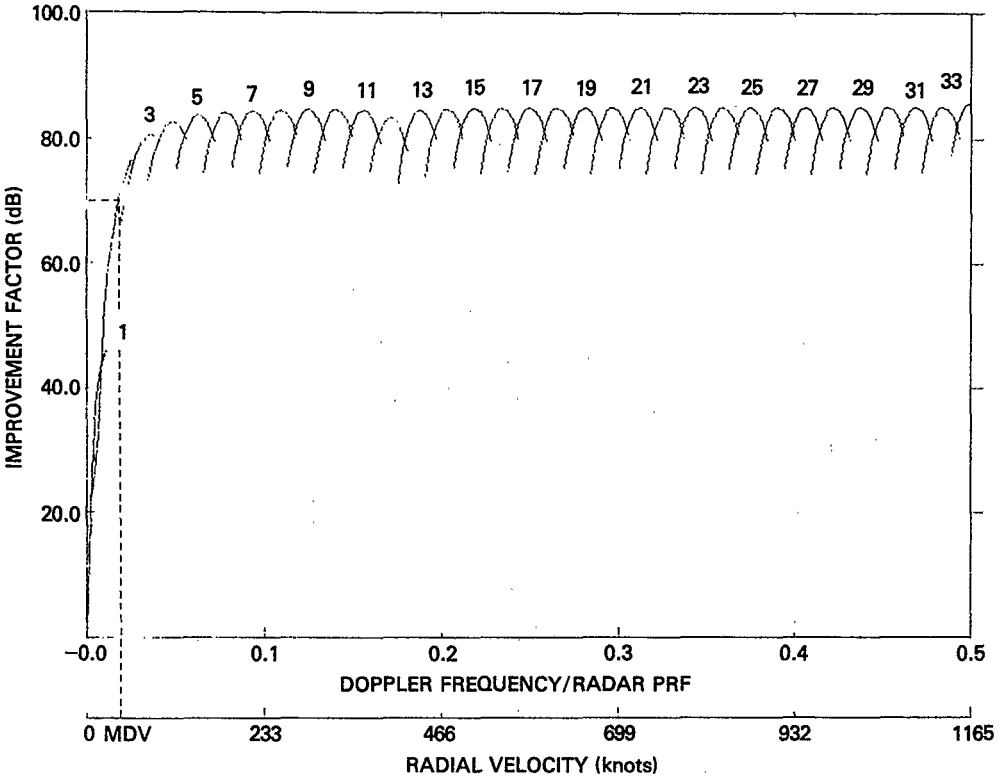

Fig. 7 — Improvement factor for a DPCA canceller cascaded with a 64-pulse matched filter processor. The clutter-to-noise ratio is 65 dB.

Criteria used to evaluate the performance of a particular Doppler processor are: the improvement factor (IF), which is a measure of the clutter rejection capability; the signal processing loss, which is a measure of the loss in signal to noise ratio from the ideal; and the minimum detectable velocity (MDV), which is a measure of the ability to detect low velocity targets or targets whose velocity vector is nearly tangential to the direction of the radar.

The limitations and disadvantages of the former processors are primarily in the areas of the signal processing loss and MDV response.

Feedback MTI

The conventional MTI canceller delays the returns of a given transmitted pulse and subtracts them from the returns of the next transmitted pulse. N cascaded cancellers are equivalent to an $(N + 1)$ sample transversal filter with weights corresponding to the Nth-degree bionomial coefficients with alternating signs [5].

In general, the binomial weights are

$$w_i = (-1)^i \begin{bmatrix} N_c \\ i \end{bmatrix}, \quad i = 0, 1, \ldots, N_c \tag{17}$$

where $\begin{bmatrix} N_c \\ i \end{bmatrix} = \dfrac{N_c!}{i!(N_c - i)!}$ and N_c is the number of cancellers.

For a triple canceller ($N = 3$), the binomial weights would be (1, −3, 3, −1), which when normalized by dividing by the absolute value of the largest binomial coefficient would be (0.333, −1.0, 1.0, −0.333).

Figure 8 shows the filter gain relative to the maximum filter gain vs Doppler frequency relative to the radar pulse repetition frequency (PRF) for 1 to 7 MTI cancellers [2].

By cascading MTI cancellers the clutter-rejection null (centered around 0 and 1 on the horizontal axis) is broadened as shown by Fig. 8. For a given clutter spectral distribution, the broader null yields a better IF as shown by Fig. 9. The penalty paid for the gain in the IF is a poor MDV response [8] as well as wide blind velocity regions that occur when the Doppler frequency is a multiple of the PRF.

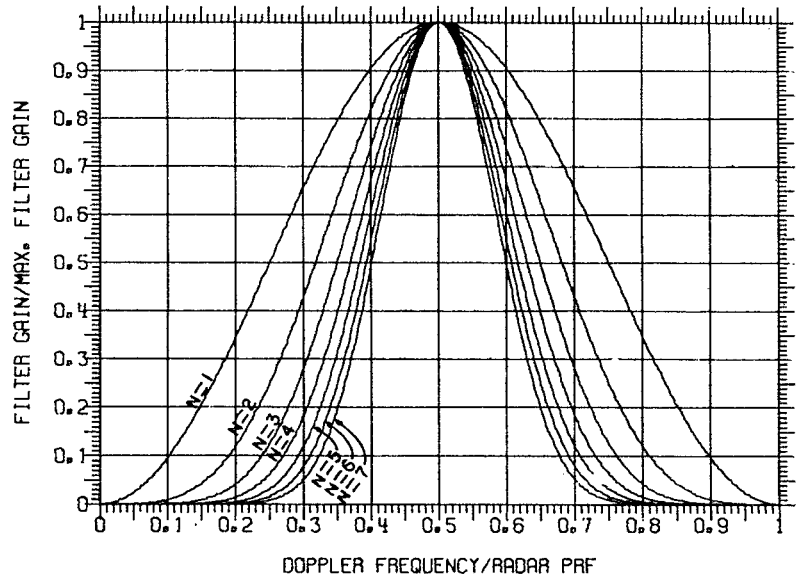

Fig. 8 — Normalized power transfer function for an MTI having the indicated number of cancellers

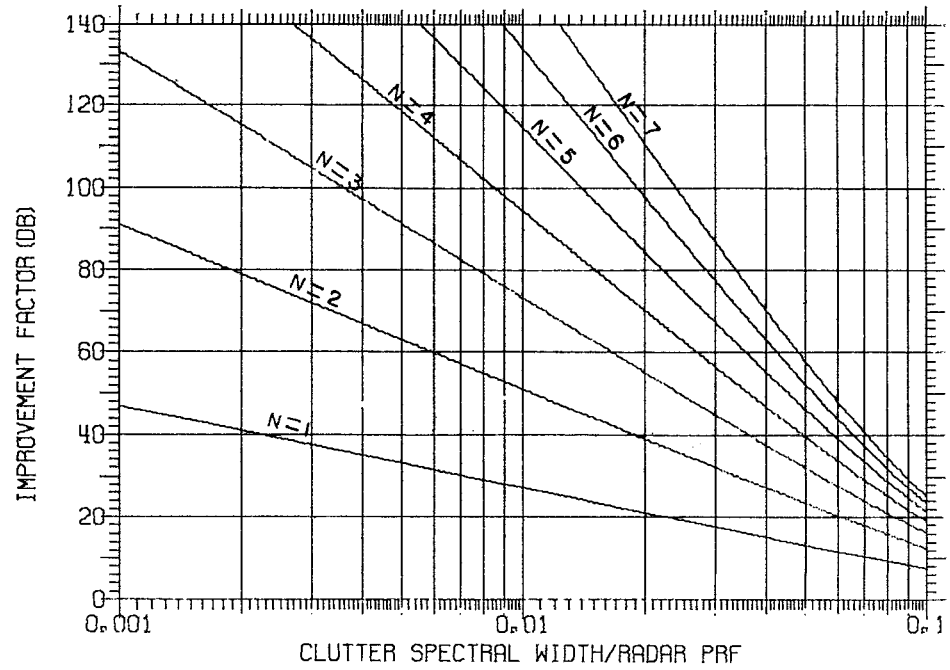

Fig. 9 — Improvement factor (IF) for an MTI having the indicated number of cancellers (filters)

Another concurrent problem with the poorer MDV response is the increase of the loss (Fig. 10) as the number of cancellers cascaded increases where

$$\text{Loss} = 10 \log (N_c + 1). \tag{18}$$

The loss corresponds to the loss of an MTI. However, if the MTI is followed by coherent or noncoherent integrators, this loss can be reduced, but not eliminated.

One method of improving the poor MDV response of the MTI is by shaping the *skirt* of the filter by various weighting schemes as shown, for example, in Fig. 11 from [9] where $1/T$ is equal to the PRF. This method improves the MDV response but the shaping requires longer processing times (which implies more pulses processed) which in turn increases the loss.

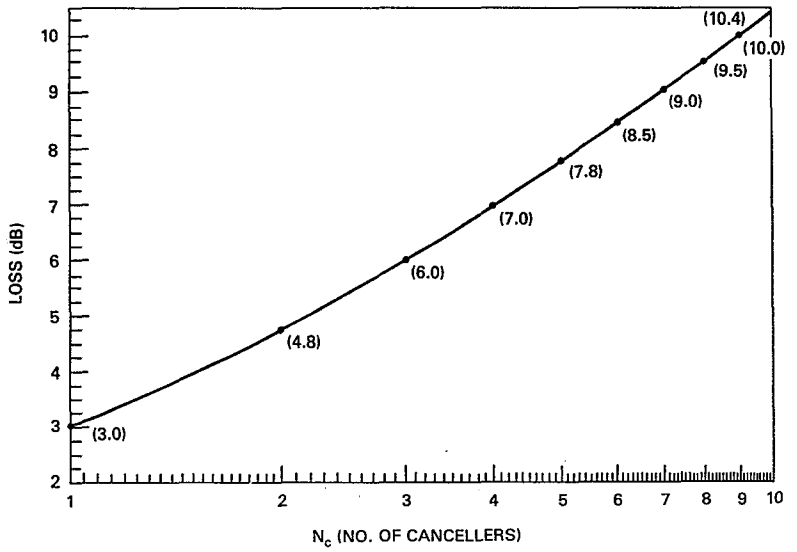

Fig. 10 — Loss for an MTI having the indicated number of cancellers

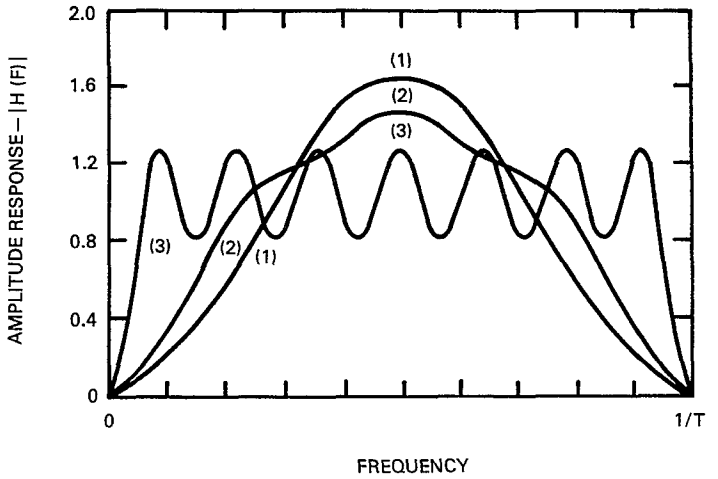

Fig. 11 — Amplitude responses for three MTI delay-line cancellers. (1) Classical 3-pulse canceller, (2) 5-pulse delay-line canceller with "optimum" weights, and (3) 15-pulse Chebyshev design. (After Houts and Burlage [9].)

Coherent Integrator (FFT)

The weighted FFT gives a better MDV response than the MTI [2, 8], but it also produces 2 to 3-dB losses because of the weighting function which lowers the filters' sidelobes everywhere, not just in the vicinity of the clutter (see Fig. 12).

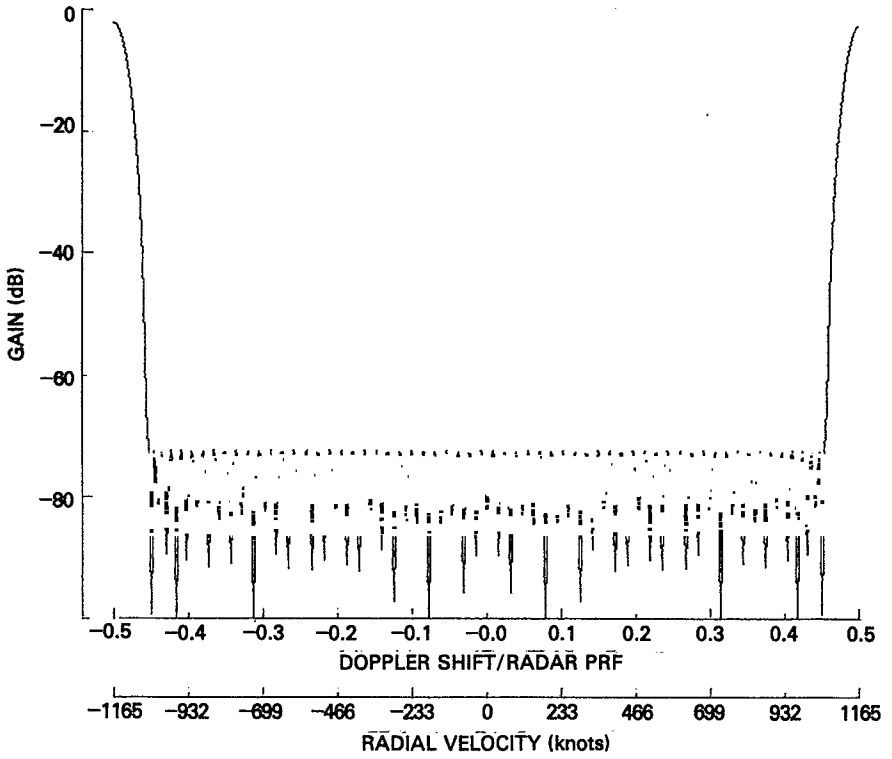

Fig. 12 — Filter No. 33 of a 64-pulse FFT with −70 dB Chebyshev-weights — loss ≈ 2.2 dB

Heavy weighting (to control the level of the sidelobes) is needed for the required IF. The result is a wider main lobe with its concurrent poorer MDV response because the filters closer to the main lobe clutter reject less clutter causing the output clutter residue to be dominated by the main lobe clutter. The effect of this domination is a reduced detectability for the low velocity targets in the filters close to the main lobe clutter [8].

For comparison with the matched filter processors formerly presented, Fig. 12 shows filter number 33 of a 64-pulse FFT with −70 dB Chebyshev weights (chosen as a result of the required IF of 70 dB). The loss is about 2.2 dB.

The IF for a 64-pulse FFT with a clutter-to-noise ratio of 65 dB and −70-dB sidelobes is shown in Fig. 13. The IF for filter number 33 is about 75 dB; the MDV is about 120 knots.

Figure 14 shows the input and output spectra of filter number 33 for the FFT 64-pulse processor. The figure shows that the output spectrum is still dominated by the main lobe clutter residue. We can further reduce the main-lobe clutter residue by preceding the FFT processor with one or more moving target indicators (MTIs).

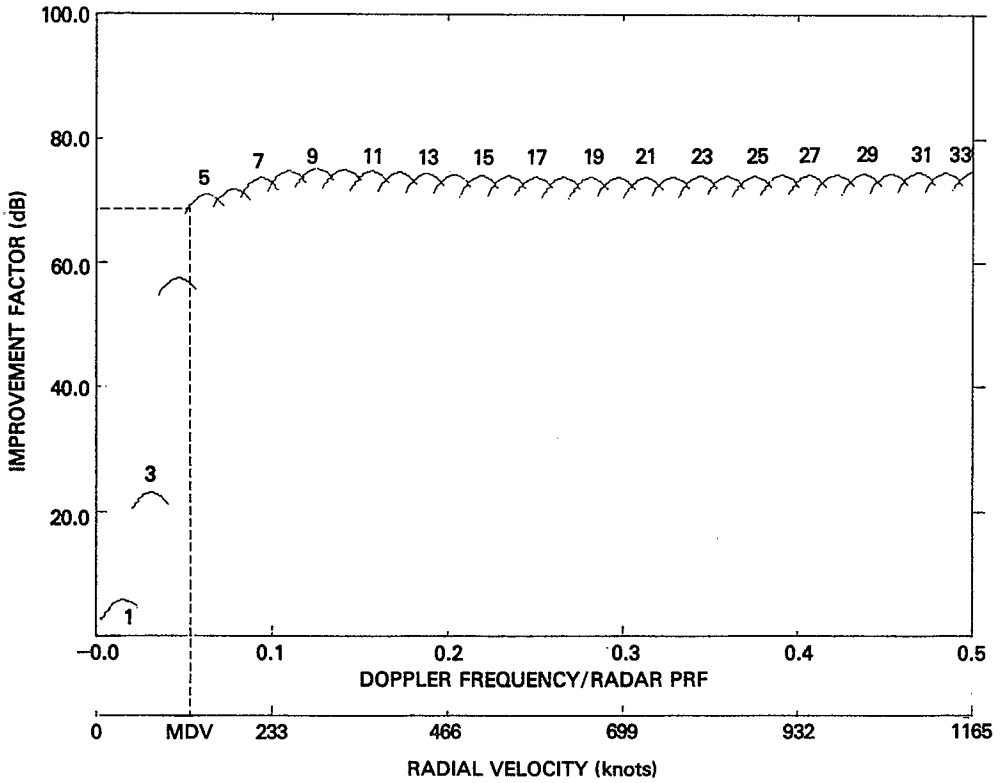

Fig. 13 — Improvement factor for a 64-pulse coherent integrator (FFT) with sidelobe clutter at the −70 dB level and clutter-to-noise ratio of 65 dB

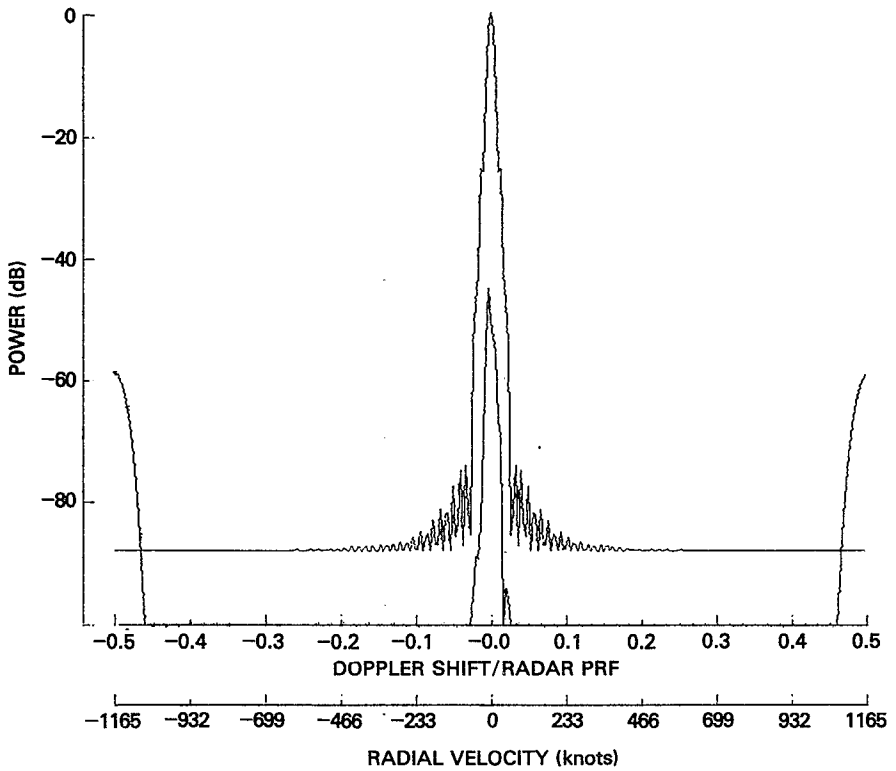

Fig. 14 — Input and output spectra of filter No. 33

Cascaded MTI and FFT

The performance of coherent integrators against *white* noise is well established. Since the performance in *colored* noise (or clutter) is irregular and unpredictable [2], we will partially *prewhiten* the clutter input to the coherent integrator by preceding it with an MTI canceller.

Figure 15 shows the IF for a double-canceller MTI cascaded with a 64-pulse FFT with uniform weights. With uniform weights, the loss is less than 0.1 dB. The MDV is increased to about 170 knots due to the poor MTI low velocity response.

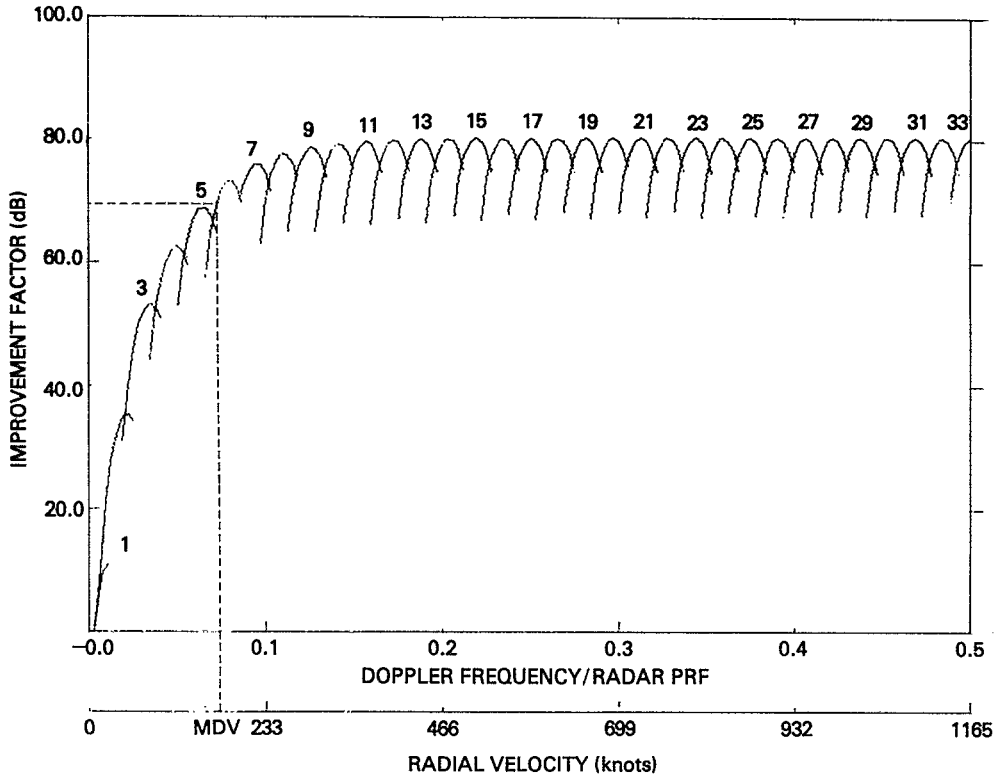

Fig. 15 — Improvement factor for a double-canceller MTI cascaded with a 64-pulse coherent integrator with uniform weights (unweighted)

DESIGN PROCEDURE

The matched filters could be designed to give the best performance by computing the weights for the clutter spectrum at each antenna pointing angle. This would probably need to be implemented adaptively. An alternative method would be to compute a finite number of sets of weights at specific angles (e.g., 0°, 45°, and 90°). The set corresponding to the angle closest to the horizontal pointing angle could then be picked and used. The Doppler spectral spreading due to range ambiguities can be compensated for with quadratic phase modulation. However, for this analysis we will take only a single range cell.

The matched filters of the example presented here were designed for the widest clutter spectrum and highest clutter-to-noise ratio (CNR) expected. The worst case weights (i.e., for a horizontal pointing angle of 90° which maximizes the effects of platform motion) were computed and stored. These weights were then used at all other horizontal pointing angles.

Figure 16 shows the target outputs of an airborne radar model (Xs) superimposed on the matched filter improvement factor curves for the worst case mentioned above. The radial velocities of the targets that were modeled were selected to be at the center of filters 2, 3, 4, 5, 7, 9, 17, and 33. The horizontal pointing angle for both outputs was 90°. The CNR for both outputs was 65 dB. As shown in Fig. 16, the modeled outputs match the filter responses rather well. The circled, modeled output represents the performance using the skirt of filter 3 rather than the center of filter 2 for the target that is centered in filter 2. Since the skirt of filter 3 (in this case) outperforms filters 1 and 2, a good case could be made for discarding the results of filters 1 and 2 (and also filter 64).

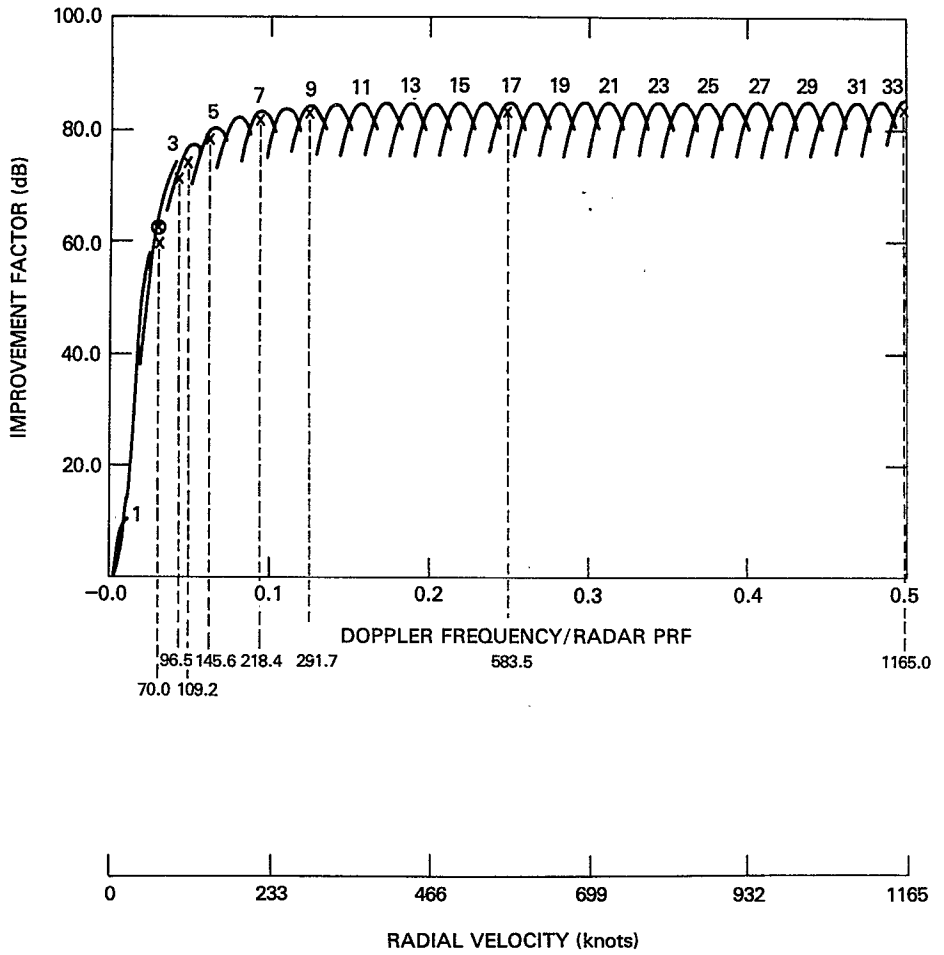

Fig. 16 — Matched filter modeled target outputs (Xs) superimposed on the matched filter improvement factor curves. The horizontal pointing angle is 90° (for both targets and filter design). The clutter-to-noise ratio is 65 dB (for both targets and filter design).

Figure 17 shows the modeled outputs with a 55-dB CNR. Both outputs still represent a 90° horizontal pointing angle. The IF is about 10 dB less. However, the IF for filter 2 is about the same (i.e., about 60 dB). With a CNR of 55 dB we require 10 dB less cancellation (i.e., 60 dB rather than 70 dB). We can conclude that our matched filter processor using the 90° weights and designed for a 65-dB CNR performs at least as well in terms of the MDV against the 55-dB CNR clutter as it did against the 65-dB CNR clutter.

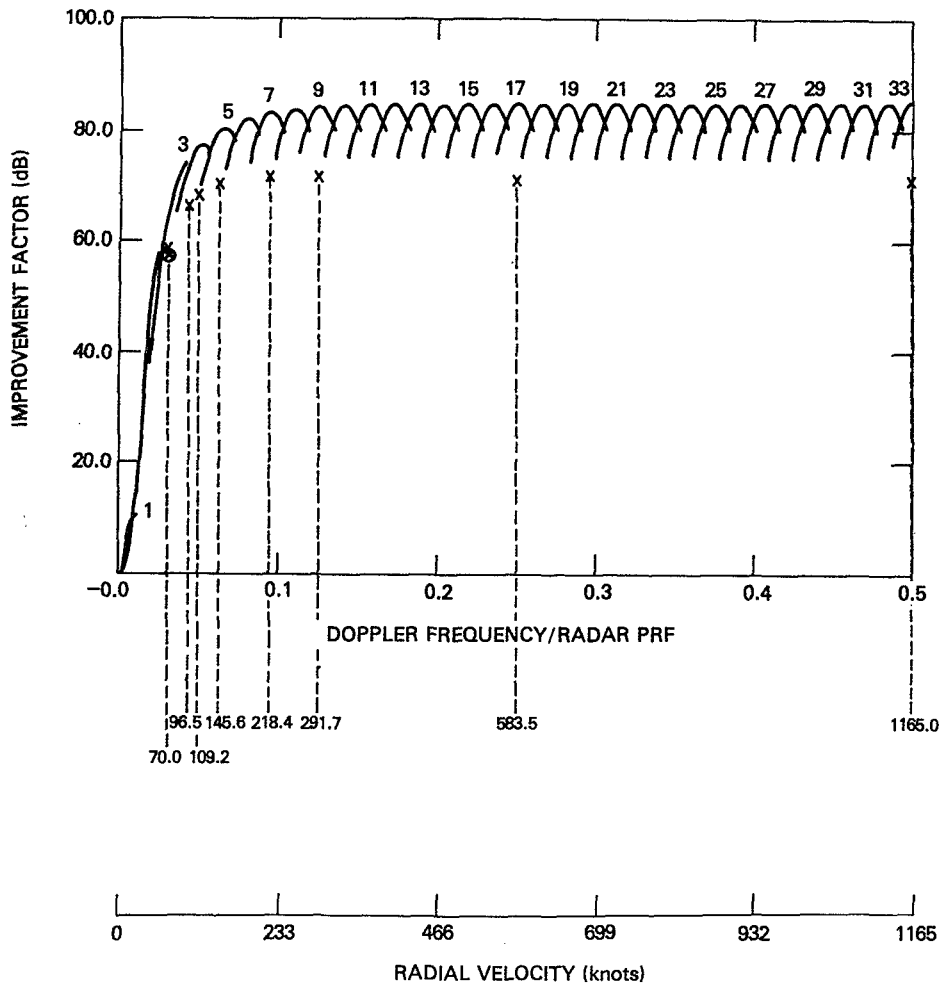

Fig. 17 — Modeled target output (Xs) superimposed on the improvement factor curves. The horizontal pointing angle is 90° (for both targets and filter design). The clutter-to-noise ratios are 55 dB (targets) and 65 dB (filter design).

Figure 18 shows the modeled outputs with a CNR of 55 dB and a horizontal pointing angle of 0° superimposed on the filter response matched to a CNR of 65 dB and horizontal pointing angle of 90°. The IF here is essentially the same as that in Fig. 17 except for the filters near the clutter, where it is actually better if the skirt of filter 3 is used rather than the center of filter 2.

As shown by the modeled outputs in Fig. 18 where we have 10 dB less CNR and the 90° weights used at 0° horizontal pointing angle (the worst possible utilization of the worst case weights), the performance in terms of the MDV is just as good and the cancellation level required is still achieved. One can conclude then that this particular set of weights will suffice for this example. Also, we have compared the matched filter using these weights to the FFT processors earlier in this report. We found that the matched filter processor outperforms these configurations without adapting the weights for each antenna pointing angle. Therefore, the implementation of this processor is not significantly more complex than the FFT processors.

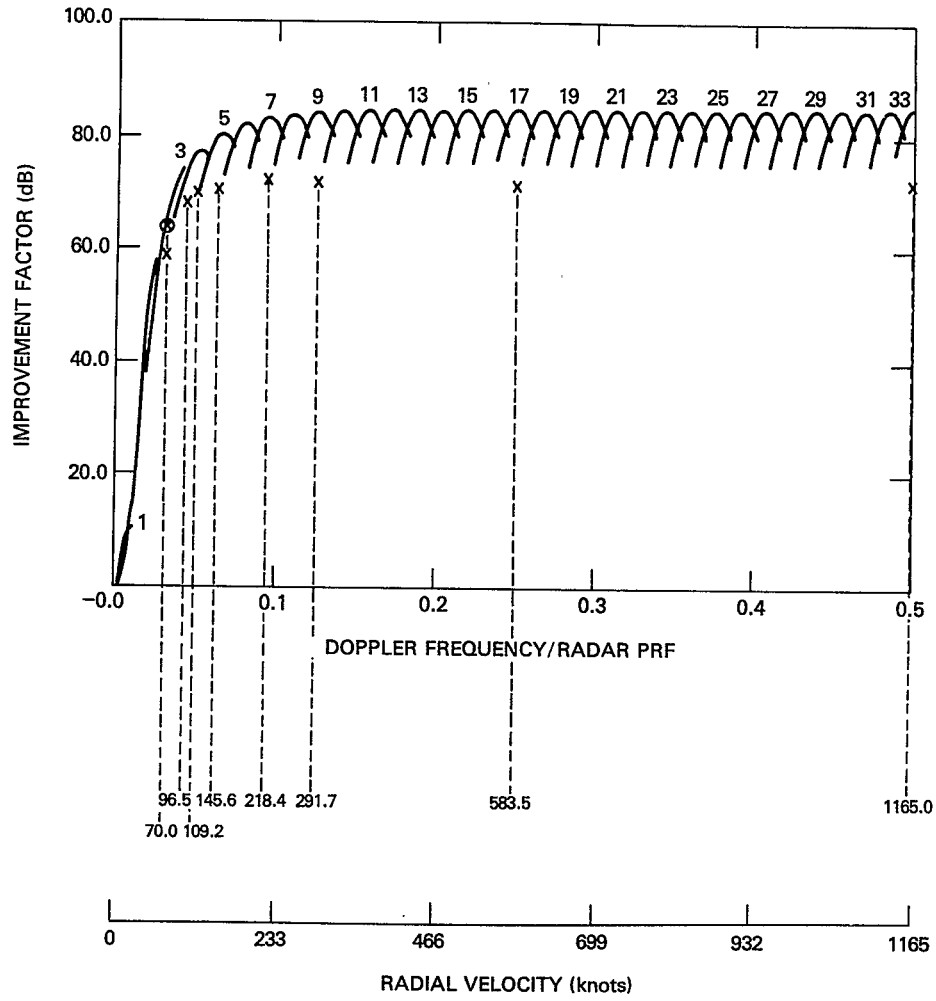

Fig. 18 — Modeled target (Xs) superimposed on the improvement factor curves. The horizontal pointing angles are 0° (targets) and 90° (filter design). The clutter-to-noise ratios are 55 dB (targets) and 65 dB (filter design).

SUMMARY AND CONCLUSIONS

We have considered five processor configurations in this research to be applied to an airborne radar:

1. FFT processor with −70 dB Chebyshev weights,
2. Double-canceller MTI cascaded with an FFT processor,
3. Single-canceller MTI cascaded with a matched filter processor,
4. Matched filter processor, and
5. DPCA-canceller cascaded with a matched filter processor.

Using a design example, our goal was to achieve 70 dB or better clutter rejection with minimal loss and a minimum detectable velocity (MDV) of 100 knots or less.

A comparison of these five configurations yields the following *approximate* results:

Type of Processor	MDV (knots)	Loss (dB)
1. FFT	120	2.2
2. MTI-FFT	170	0.1
3. MTI-MATCHED	80	0.1
4. MATCHED	80	0.1
5. DPCA-MATCHED	45	0.1

Our conclusions are:

1. 70-dB or better clutter cancellation is achievable with all configurations for our design example.

2. Configurations 3, 4, and 5 each have a low enough MDV to meet the criteria set by our design example.

3. Configurations 3 and 4 give the same results. Configuration 3 requires less processing hardware because the cancellation ratio of the MTI-canceller reduces the dynamic range required for the matched filter. Configuration 4 is a more straightforward design which is based on the spectrum due to platform motion, whereas the design of Configuration 3 is based on the platform motion spectrum after the MTI cancellation.

4. Configuration 5 produced the lowest MDV with overall results as good as the other configurations but Configuration 5 requires three antenna patterns to be generated which complicates the antenna design.

5. In Configuration 4, the filters were matched to a wide clutter spectrum (at broadside) and performed at least as well for a narrow clutter spectrum (straight-ahead) in terms of the MDV. If the filters were perfectly matched we could achieve a better signal-to-noise ratio (a reduced loss), but the difference between such a reduced loss and the 0.1-dB loss of our design example would be insignificant for most applications, especially when the added complications are considered.

6. The primary motive for implementing Configuration 4, the matched filter processor, is its simplicity and the fact that only one set of weights needs to be computed and applied at all pointing angles.

REFERENCES

1. G.A. Andrews, Jr., "Comparison of Radar Doppler Filtering Techniques," NRL Report 7811, October 17, 1974.

2. G.A. Andrews, Jr., "Performance of Cascaded MTI and Coherent Integration Filters in a Clutter Environment," NRL Report 7533, March 27, 1973.

3. S.P. Applebaum, "Adaptive Arrays," SPL-769, Syracuse University Research Corp., June 1964.

4. L.E. Brennan and I.S. Reed, "Theory of Adaptive Radar," *IEEE Trans.* AES-9(2), 237-252, Mar. 1973.

5. G.A. Andrews, Jr., "Optimal Radar Doppler Processors," NRL Report 7727, May 29, 1974.

6. G.A. Andrews, Jr., "Airborne Radar Motion Compensation Techniques: Evaluation of TACCAR," NRL Report 7407, Apr. 12, 1972.

7. G.A. Andrews, Jr., "Airborne Radar Motion Compensation Techniques: Optimum Array Correction Patterns," NRL Report 7977, March 16, 1976.

8. G.A. Andrews, "An Airborne Radar Doppler Processing Philosophy," NRL Report 8073, January 31, 1977.

9. R.C. Houts and D.W. Burlage, "Design Procedure for Improving the Usable Bandwidth of an MTI Radar Signal Processor," IEEE Conference Record 1976 International Conference on Acoustics, Speech, and Signal Processing, April 12-14, 1976, Phila., Pa., IEEE Cat. No. 76CH1067-8 ASSP.

Appendix
AIRBORNE RADAR CLUTTER MODEL

Clutter Spectrum

For an airborne radar, curves of constant Doppler shift (isodops) can be determined by the Doppler frequency equation

$$f_d = \frac{2v_p}{\lambda} \cos \beta, \tag{A1}$$

where f_d represents the Doppler frequency, v_p is the magnitude of the platform velocity vector, λ is the transmitted wavelength, and β is the angle measured from the velocity vector to the line of sight of an earth point (Fig. A1). From the coordinate system defined in Fig. (A1),

$$\cos \beta = \cos D \cos \phi \cos \alpha + \sin D \sin \phi, \tag{A2}$$

and

$$f_d = \frac{2v_p}{\lambda} (\cos D \cos \phi \cos \alpha + \sin D \sin \phi). \tag{A3}$$

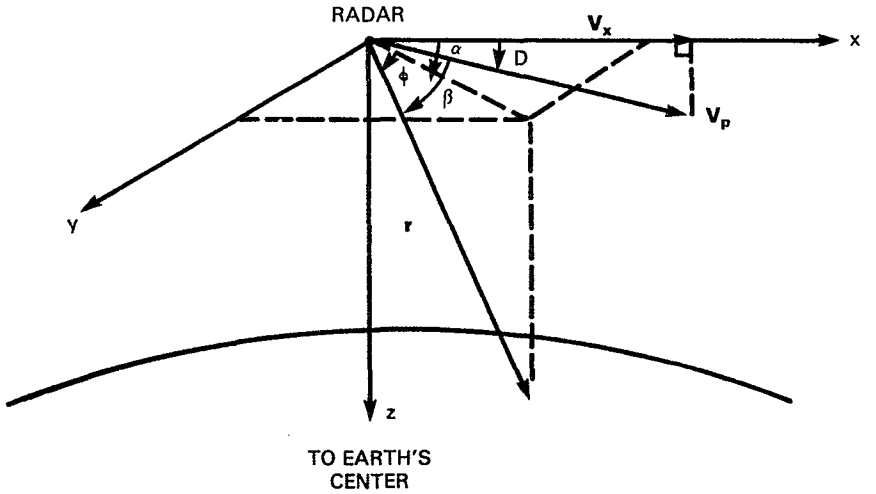

Fig. A1 — Geometry of an airborne radar showing the relationship of azimuth angle (α), depression angle (ϕ), and dive angle (D)

In modeling the clutter, isodops are determined by Eq. (A3). The total clutter level in a given Doppler filter is determined by summing the clutter in the ambiguous range cells along the isodop centered on the filter. The isodops centered on the filters are determined by using frequency steps of $\Delta f_d = \frac{1}{NT}$ where T is the interpulse period and N is the number of pulses to be processed.

Figure A2 shows the isodops for 64 filters and 0° dive angle. Outermost circles represent the horizon for a 5 nmi (30 000 ft) altitude. The radar platform's velocity vector points toward the top of the figure. The frequency for zero azimuth and zero dive angle is

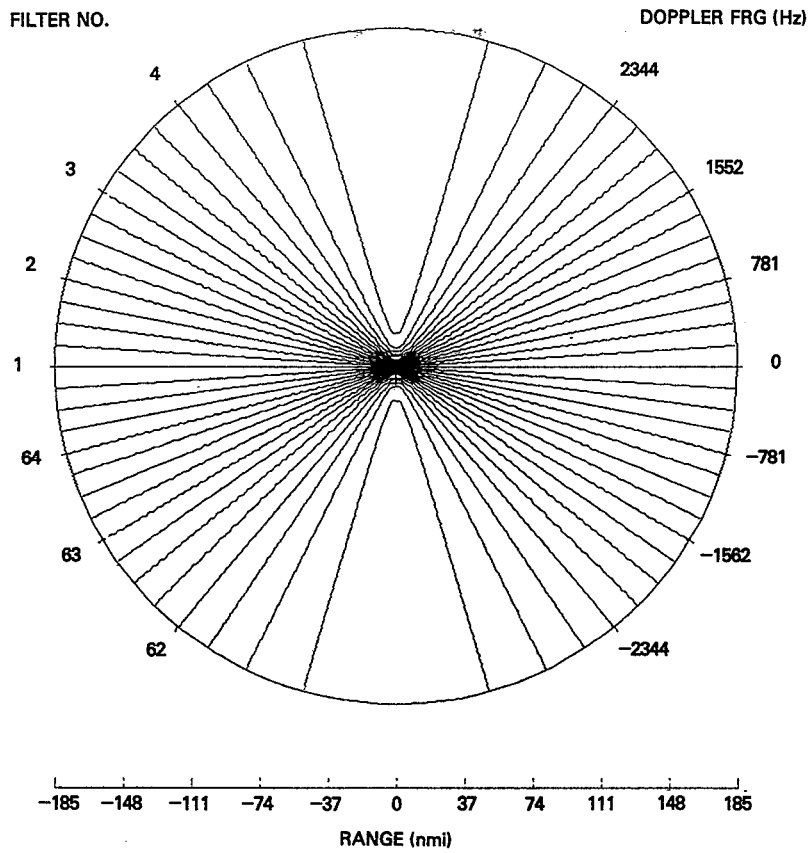

Fig. A2 — Isodops for a 5 nmi (30 000 ft) altitude, 0° dive angle and 64 filters; the transmit frequency is 3 GHz; and the PRF is 50 kHz

$$f_0 = \frac{2v_p}{\lambda} \cos \phi. \tag{A4a}$$

For 180° azimuth and zero dive angle the frequency is

$$f_{180} = -\frac{2v_p}{\lambda} \cos \phi. \tag{A4b}$$

In our case the azimuth of the antenna is 90°, v_p = 300 knots, λ = 0.1 m, and ϕ = 4.3° (corresponding to a 3° grazing angle).

Substituting these values in Eq. (A4a) gives a frequency at zero azimuth of 3080 Hz (−3080 at 180° azimuth). The frequency at 90° azimuth and zero dive angle by Eq. (A3) is 0.0 Hz.

Also for our case, $\Delta f_d = \frac{1}{NT}$ gives Δf_d = 781 Hz where N (the number of pulses processed) is 64, $T = 2 \times 10^{-5}$ s (i.e., PRF = 50 kHz).

The frequency feeding into a filter is computed by

$$f_j = n\Delta f_d \tag{A5}$$

where

$$n = \text{INT}(f_{180}), \ldots, -2, -1, 0, 1, 2, \ldots, \text{INT}(f_0),$$

and

$$j = (n + 1) \text{ modulo } (N).$$

Since INT $\left(\frac{3080 \text{ Hz}}{781 \text{ Hz}}\right)$ is 3, there are seven filters such that $\frac{-2v_p}{\lambda} \cos \phi \leqslant f_j \leqslant \frac{2v_p}{\lambda} \cos \phi$ (i.e., there are seven filters that contain clutter). In our case $n = -3, -2, -1, 0, 1, 2, 3$. Filter 1 is centered at 0.0 Hz, filter 2 at ($j = 2$, $n = 1$) 781 Hz, filter 3 at ($j = 3$, $n = 2$) 1562 Hz, and filter 4 at 2343 Hz. Filter 5 would be at 3124 Hz, but since the frequency at 0° azimuth is 3080 Hz (for this case), there is no filter 5. Also by symmetry (in this case), filters 64, 63, and 62 are centered at −781 Hz, −1562 Hz, and −2343 Hz, respectively.

As shown by Fig. A2 equal steps in frequency (Δf_d) produce unequal angular steps.

In the example presented here, only seven filters (1, 2, 3, 4, 62, 63, and 64) centered around zero Doppler contain clutter as shown by Fig. A2.

Figure A3 shows the two-way circular antenna pattern used. It has a 1.5-m aperture with uniform weights on transmit, 34-dB truncated Gaussian weights on receive, and a nominal frequency of 3 GHz.

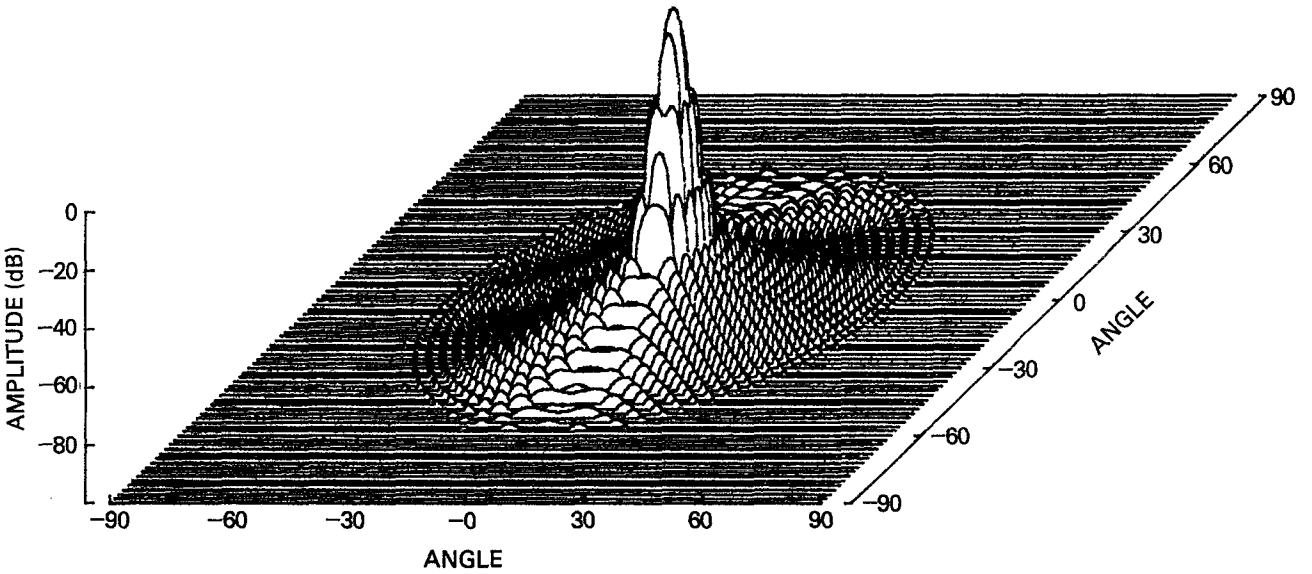

Fig. A3 — Two-way circular antenna pattern with a 1.5-m aperture, uniform weights on transmit, 34-dB truncated Gaussian weights on receive, and frequency of 3 GHz

To get the clutter contribution along an isodop we must sum over many ambiguous slant-ranges.

To determine the clutter level in each range-gate we sum the contribution at all azimuth angles received along a constant slant-range cell plus all ambiguous slant-range cells (we have a range ambiguous waveform).

The ambiguous range-gates with equal slant-range increments corresponding to a 50 kHz PRF are shown in Fig. A4. When Fig. A4 is compared with Fig. A2, it is evident that there are many different Doppler frequencies at each particular slant-range.

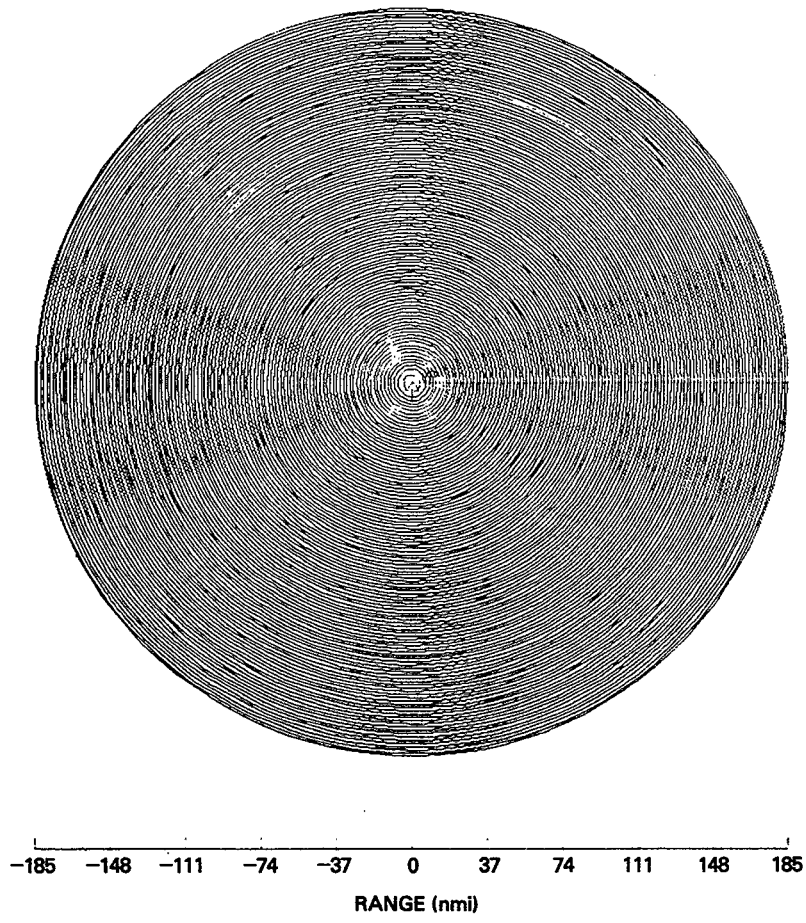

Fig. A4 — Ambiguous range gates for a 5 nmi (30 000 ft) altitude and PRF of 50 kHz

Therefore, to model the clutter, vertical angles relative to the antenna depression angle of the beam center are computed for each ambiguous slant-range cell starting with the minimum ambiguous slant-range cell.

Azimuth points relative to the horizontal pointing angle of the antenna are then computed for each point on the circular antenna pattern (Fig. A3). Each different depression angle has this set of azimuth points.

The amplitude of each clutter sample is computed for each point on the antenna pattern. The amplitude consists of the gain of the antenna pattern at that angle and the radar cross section of the clutter which has a Rayleigh distribution in this example.

Next the Doppler frequency for each clutter sample is determined by Eq. (A3). The total clutter amplitude at a given Doppler frequency is determined by summing the amplitudes of all of the clutter samples with the given Doppler frequency in a selected slant-range cell. This includes all of the ambiguous slant-ranges of the selected slant-range cell.

After correcting for platform motion by a TACCAR processor technique [A1], the amplitudes for each Doppler frequency can be plotted to construct the clutter spectrum (Fig. 2).

Clutter Level

According to Skolnik [A2],

$$\theta_{3\,\mathrm{dB}} = \frac{58.5\,\lambda}{a} \tag{A6}$$

for a circular distribution, where λ is the transmitted wavelength, a is the aperture width, and $\theta_{3\,\mathrm{dB}}$ is the half-power beamwidth in degrees.

By Nathanson [A3], the area of the clutter is

$$A_c \cong \frac{c\tau}{2} \sec \psi \left[2R \tan\left(\frac{\theta_{3\,\mathrm{dB}}}{2}\right)\right], \tag{A7}$$

where R is the slant-range to the center of the clutter cell, τ is the pulse width, c is the propagation speed, and ψ is the grazing angle.

The slant-range is determined by

$$R = R_p \sin\phi - \sqrt{R_e^2 - R_p^2 \cos^2\phi}, \tag{A8}$$

where

$$R_p = R_e + h. \tag{A9}$$

Here, h is the altitude, R_e is the earth's radius, and ϕ is the depression angle of the earth point with slant-range R.

To compute the total clutter cross-section,

$$\sigma_c = A_c \sigma^0 N_a, \tag{A10}$$

where σ_c is the total clutter cross-section, σ^0 is the clutter cross-section per unit area, and N_a is the number of slant-range ambiguities.

The signal to clutter ratio is

$$\frac{s}{c} = \sigma_t/\sigma_c = \frac{\sigma_t}{A_c \sigma^0 N_a}.$$

$$\left(\frac{s}{c}\right)_{\mathrm{dB}} = (-\sigma^0)_{\mathrm{dB}} - 10 \log A_c - 10 \log N_a + (\sigma_t)_{\mathrm{dB}}, \tag{A11}$$

where σ_t is the target mean radar cross-section.

In our example we consider an S-band (3 GHz) radar with a 1.5-m aperture at an altitude of 5 nmi (30 000 ft). The range resolution ($c\tau/2$) is 90 m (300 ft). For this case, $N_a = 102$, $\lambda = 0.10$ m, $a = 1.5$ m, $\psi = 3°$, and $\sigma_t = 13$ dBsm.

Equation (A6) produces $\theta_{3\,\mathrm{dB}} = 3.90°$. Equation (A7) gives

$$A_c \cong 0.26 \text{ nmi}^2 \ (9.08 \times 10^5 \text{ m}^2).$$

Equations (A10) and (A11) produce

$$\left(\frac{s}{c}\right)_{\mathrm{dB}} = (-\sigma^0)_{\mathrm{dB}} - 67 \text{ dB}.$$

Table A1 summarizes the results for various clutter types where SCR is the signal to clutter ratio. Our goal in this research was a 70 dB improvement factor (IF).

Table A1 — Clutter Estimation

Clutter Type	σ^0 (dB, M^2/M^2)*	Grazing Angle	SCR (dB)	Req. IF (dB)
Sea	−46	3°	−21	34
Desert	−40	10°	−27	40
Farmland	−33	10°	−34	47
Woods	−26	10°	−41	54
Cities	−18	10°	−49	62

*Reference A3, pp. 235, 263

REFERENCES

A1. G.A. Andrews, Jr., "Airborne Radar Motion Compensation Techniques: Evaluation of TACCAR," NRL Report 7407, Apr. 12, 1972.

A2. M.I. Skolnik, *Introduction to Radar Systems*, 2d ed., McGraw-Hill, New York, 1980.

A3. F.E. Nathanson, *Radar Design Principles; Signal Processing and the Environment*, McGraw-Hill, New York, 1969.